2D Mixed Halide Perovskites for Ultraviolet Light-emitting Diodes

*Manchen Hu,[1†] Junrui Lyu,[1†] Natalia Murrietta,[1†] Sebastian Fernández,[1] William Michaels,[1] Qi Zhou,[1] Pournima Narayanan,[1,2] Daniel N. Congreve[1]**

1: Department of Electrical Engineering, Stanford, CA 94305, USA.
2: Department of Chemistry, Stanford, CA 94305, USA.
*: Corresponding author email: congreve@stanford.edu
†: These authors contributed equally to this work

Abstract:

Advances in perovskite light-emitting diodes (PeLEDs) have established them as viable candidates for next-generation displays and lighting across the entire visible spectrum, with recent investigations extending their emissive properties into the deep blue and violet regions. These materials have the potential to overcome the fabrication complexities inherent in conventional III-V semiconductors by circumventing the necessity for lattice-matching, instead allowing for straightforward deposition of polycrystalline films without relying on metal-organic chemical vapor deposition. However, achieving shorter emission wavelengths presents a significant challenge due to the larger bandgaps required of both the perovskite and charge transport materials, compounding the difficulty in managing electron-hole pair recombination dynamics necessary for efficient electroluminescence. In this work, we address these challenges by precisely tuning the halide composition in two-dimensional perovskites, successfully extending the bandgap to 3.1 eV and achieving photoluminescent emission at 393 nm. By introducing an optimized dual electron transport layer architecture, we improve electron injection and hole confinement within the perovskite matrix, culminating in a high-purity electroluminescent emission at 399 nm. This strategy yields a maximum external quantum efficiency of 0.16%, a new benchmark for PeLEDs operating in this spectral domain. These findings highlight the potential of large bandgap perovskite materials for next-generation light-emitting applications.

Keywords: Ultraviolet; 2D Materials; Metal Halide Perovskite; Light-Emitting Diodes; Electron Transport Layer

Ultraviolet (UV) light, with its potent germicidal properties, is essential for sterilization in healthcare and food safety, and drives advancements in data technology, 3D printing, nanofabrication, and optical communication systems.[1,2,3-5] Despite its ubiquitous use, the development of UV light-emitting diode (LED) technology faces significant challenges, primarily dominated by the complex manufacturing processes associated with III-V semiconductors including InGaN, GaN, and AlGaN materials.[1] These traditional methods rely on strict lattice matching and epitaxial growth, often necessitating the use of metal-organic chemical vapor deposition (MOCVD), which involves high-temperature toxic precursor gases.

The advent of metal halide perovskites and their extraordinary optoelectronic properties have revolutionized the field of light-emitting diodes.[2–10] These materials are celebrated for their ease of processing, tunable bandgaps, high luminescence efficiency, and narrow emission linewidths, positioning perovskite light-emitting diodes (PeLEDs) as promising alternatives for display and lighting technologies. In less than a decade, PeLEDs have achieved external quantum efficiencies (EQEs) exceeding 25% for green and red emissions.[3,5,11–13] Additionally, blue PeLEDs, which demand larger bandgap semiconductors, are on the cusp of achieving EQEs greater than 20%.[14–18]

Substantial progress has also been made in developing novel materials with wider bandgaps, facilitating the transition towards deep blue and violet emission.[19–26] Jin *et al.* reported using the 2D perovskite 2-phenylethylammonium ($C_6H_5CH_2CH_2NH_3^+$, PEA) lead bromide (PEA_2PbBr_4) to achieve color-pure violet LEDs with 0.04% EQEs.[20] By adapting electric-field-deposition techniques, Jie *et al*. achieved deep blue LEDs with 0.31% EQEs.[19] Besides 2D perovskites, 3D perovskite nanocrystals have also been explored for deep blue and violet devices. By synthesizing $CsPbCl_3$ nanocrystals with phenylphosphonic dichloride ($PhPOCl_2$), Qi *et al.* developed bright and stable $CsPbCl_3$ nanocrystals and fabricated violet LEDs with peak emission at 405 nm and 0.18% EQEs.[24] Regarding lead-free perovskites, Shan *et al.* synthesized $Cs_3Sb_2Br_9$ quantum dots and achieved violet LEDs with 0.21% EQEs.[21] Previously, our group improved the 2D perovskite crystallization process and produced violet LEDs with EQEs of 0.41% at 408 nm.[22]

Despite this progress, solution processed PeLEDs that can efficiently emit in the UV region has remained a challenging goal. The endeavor towards UV PeLEDs imposes even stricter requirements for larger bandgaps in perovskite emitting materials and poses heightened challenges in the design of charge transport layers and the management of radiative recombination and energy transfer. In this work, we present PeLEDs based on a 2D perovskite, which achieves a single electroluminescence (EL) peak below 400 nm with a peak EQE of 0.16%. This effort not only validates the feasibility of UV perovskite LEDs but also provides device design rules to ensure color-pure and efficient perovskite light emission.

Demonstration of Perovskite Thin Films with UV Photoluminescence

Building on our previous work studying PEA_2PbBr_4 violet emitting perovskites and taking advantage of the perovskites' tremendous halide tunability, we replaced 50% phenethylammonium bromide (PEABr) with phenethylammonium chloride (PEACl). The molar ratio of the perovskite precursors with PEACl, PEABr and $PbBr_2$, respectively, in DMSO was 1 : 1 : 1. The perovskite films were spincoated on quartz substrates and processed with a two-step annealing procedure according to our previous work.[22] More details can also be found in the Methods section. The film shows a photoluminescent (PL) spectrum peak at 393 nm with approximately a 14 nm full-width half maximum (FWHM), which is shown in Figure 1a. The perovskite films also have a strong excitonic band absorption peak at 382 nm, similar to the pure bromide 2D perovskite PEA_2PbBr_4 with an absorption peak of 402 nm.[22] According to the feed ratio, we denote our new perovskite as $PEA_2PbCl_1Br_3$. As shown in Figure 1b, we believe that $PEA_2PbCl_1Br_3$ should possess a 2D structure similar to that of PEA_2PbBr_4, where the $[PbX_6]$ (X= Cl or Br) octahedral layers are interspersed with organic PEA layers. This 2D structure is supported by X-ray diffraction (XRD) measurements. The XRD patterns in Figure 1c confirm that $PEA_2PbCl_1Br_3$ has a similar 2D structure to PEA_2PbBr_4 denoted by the signature (*001*) peaks. We also performed XRD fine scans from 4.8 to 5.8 degrees and from 15.4 to 16.4 degrees to enable detailed comparisons between $PEA_2PbCl_1Br_3$ and PEA_2PbBr_4. No obvious peak shifts are observed in these two XRD spectra (shown in Figure S1a and S1b). Considering only a small portion of Br is substituted by Cl, this partial substitution may not be sufficient to cause a noticeable change in the crystal structures as observed through XRD.

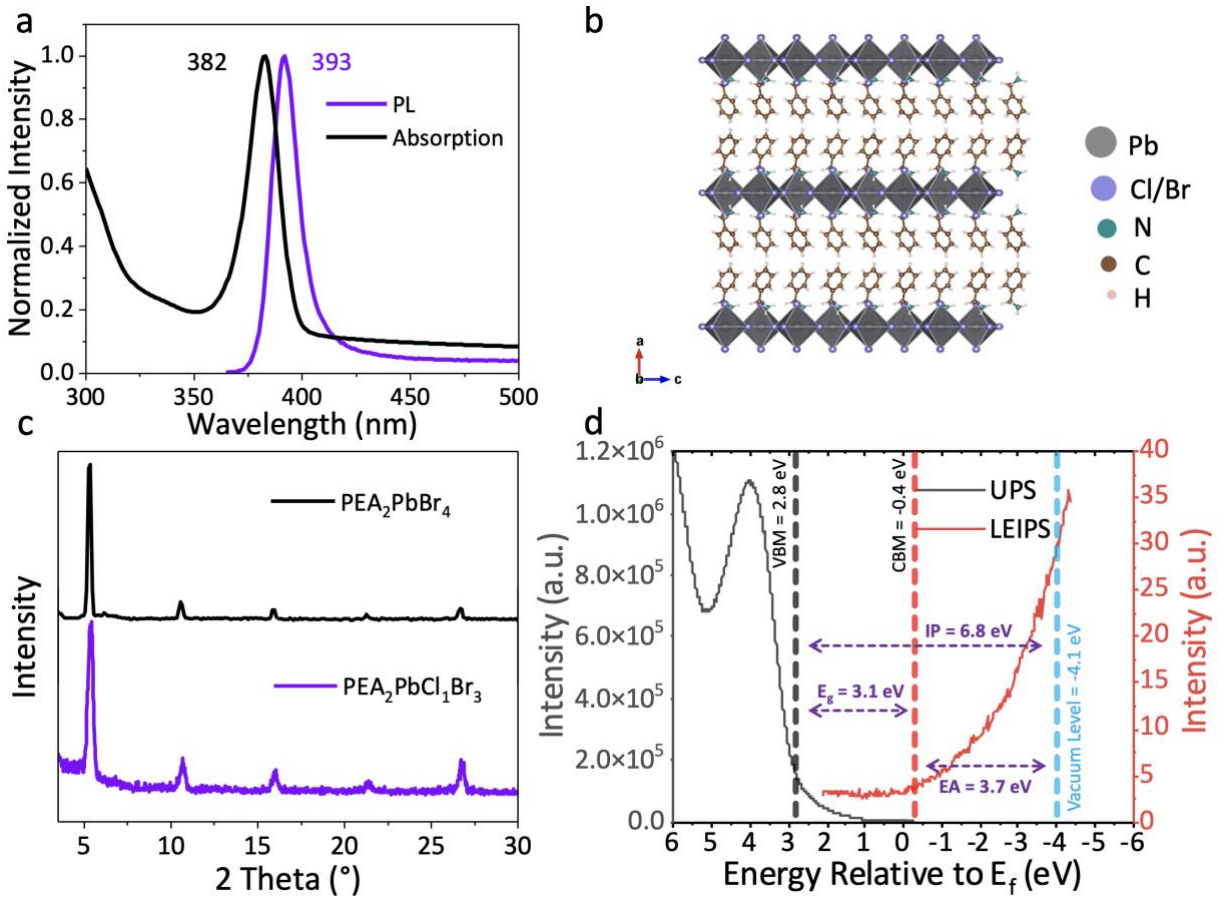

Figure 1. The optical and electronic properties of 2D perovskites.

a. The absorption spectrum and emission spectrum of the $PEA_2PbCl_1Br_3$ perovskite film under 330 nm excitation.

b. Proposed crystal structure diagram of $PEA_2PbCl_1Br_3$.

c. XRD pattern comparison of $PEA_2PbCl_1Br_3$ and PEA_2PbBr_4.

d. UPS (black) and LEIPS (red) measurement of the $PEA_2PbCl_1Br_3$ perovskite film.

To further investigate the chemical composition of the perovskite films, X-ray photoelectron spectroscopy (XPS) was employed to discern the precise atomic ratio of chlorine to bromine. As depicted in Figure S2a, the XPS spectrum allows us to elucidate the elemental constitution of the films. Furthermore, Figures S2b and S2c offer a detailed look at the binding energy regions corresponding to Pb 4f, Cl 2p, and Br 3p, respectively. Analysis of these spectra reveal that the atomic ratio within the as-synthesized perovskite films stands at Pb : Cl : Br = 21.8 : 17.3 : 60.9. This ratio aligns well with the intended stoichiometric feed ratio of Pb : Cl : Br = 1 : 1 : 3, confirming the accuracy of our fabrication process in achieving the desired chemical composition.

Emissive defect states, which are particularly prone to forming within large bandgap semiconductors, can detrimentally affect the performance of LEDs. The presence of defect states in semiconductors often manifests as changes in the PL spectrum upon varying the excitation wavelength. Figure S3 demonstrates the photoluminescence (PL) spectra of perovskite films under excitation wavelengths ranging from 260 nm to 360 nm. Notably, the consistency of the PL spectra across these excitation wavelengths suggests that $PEA_2PbCl_1Br_3$ exhibits solely band-to-band emission without significant additional radiative states. Moreover, there is only a minor contribution from red-shifted self-trapped excitons (STEs) to the PL emission. Given that $[PbCl_6]$-based perovskites are known for their broad white emission stemming from STEs,[27–29] the absence of broad emission in $PEA_2PbCl_1Br_3$ could be attributed to the predominance of bromide in the $[PbX_6]$ octahedral sites, as our synthesis involved a lower proportion of chloride substitution. This clarity in the PL spectra underscores the potential of $PEA_2PbCl_1Br_3$ as a promising candidate for UV electroluminescence (EL) applications. It should be noted that due to the relatively low photoluminescence quantum yield (PLQY) of $PEA_2PbCl_1Br_3$ (we previously measured a value of 8% for PEA_2PbBr_4)[22] and the low sensitivity of our integrating sphere in the UV wavelength region, we could not resolve accurate PLQY values of the UV films.

To ascertain the precise energy levels of the organic-inorganic hybrid 2D perovskites, we employed ultraviolet photoelectron spectroscopy (UPS) and low-energy inverse photoelectron spectroscopy (LEIPS) to probe the ionization potential (IP) and electron affinity (EA), respectively. LEIPS is particularly advantageous for its minimal chemical degradation impact on organic constituents, rendering it an optimal technique for assessing the unoccupied conduction band of organic semiconductors.[30,31] As depicted in Figure 1d, the IP was determined to be 6.8 eV using UPS. Concurrently, LEIPS facilitated the measurement of UV light emission from our sample upon exposure to low-energy electrons, enabling the calculation of an EA of 3.7 eV. Comprehensive details and calculations are presented in the supplementary materials (see Figures S4 and S5). Consequently, the bandgap of the perovskite was calculated to be 3.1 eV, corroborating the emission and absorption data presented in Figure 1a.

Investigation on Dual Electron Transport Layers

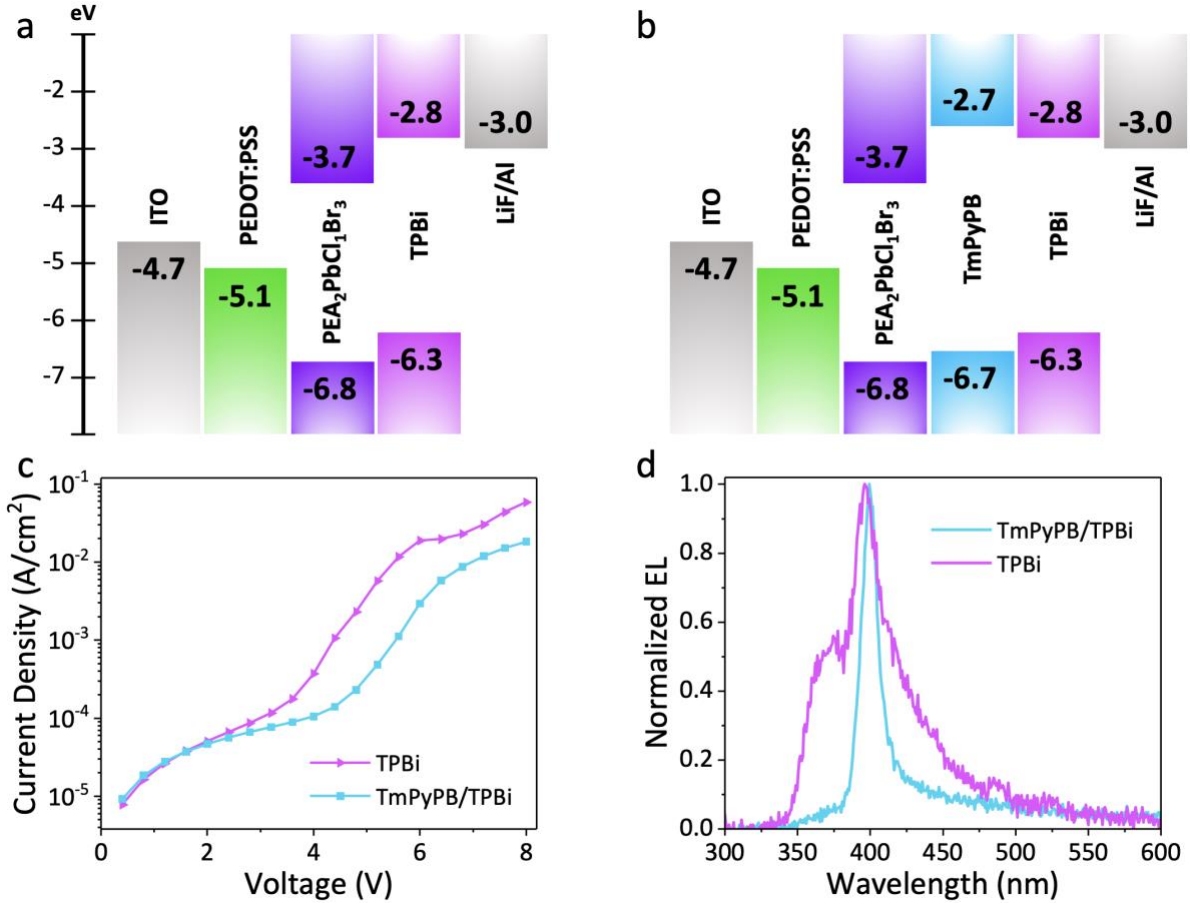

Figure 2. LED devices with different architectures.
a. Energy level diagram of the single electron transport layer device (i.e., TPBi device).
b. Energy level diagram of the dual electron transport layer device (i.e., TmPyPB/TPBi device).
c. J-V curves for the TPBi and TmPyPB/TPBi devices.
d. EL spectra of the TPBi and TmPyPB/TPBi devices show pure emission from the dual ETL architecture.

Traditional deep blue and violet PeLEDs often employ 2,2′,2″-(1,3,5-benzinetriyl)-tris(1-phenyl-1H-benzimidazole) (TPBi) as the electron transport layer (ETL) due to its favorable electronic properties.[19,20,22,25,32–35] However, as delineated by the energy level diagram in Figure 2a, TPBi's highest occupied molecular orbital (HOMO) is positioned at a higher energy compared to the valence band maximum of $PEA_2PbCl_1Br_3$. This mismatch hinders effective hole confinement within the perovskite layer, potentially facilitating hole leakage and non-radiative recombination processes. Moreover, the bandgap of TPBi, approximately 3.5 eV, is very close to the perovskite bandgap of 3.1 eV, raising concerns over emission spectral purity. The violet curve in Figure 2d illustrates the electroluminescence (EL) spectrum of a $PEA_2PbCl_1Br_3$ device with a traditional TPBi structure. When contrasted with the EL spectrum from a TPBi-only (no perovskite) device

(Figure S6), notable emission from the TPBi layer is observed, indicating excitonic recombination within TPBi that detracts from the desired device performance.

To address this challenge, we integrated an additional ETL, 1,3,5-Tri(m-pyridin-3-ylphenyl)benzene (TmPyPB), between the perovskite and TPBi layers. TmPyPB, known for its electron-deficient pyridine moieties, serves as an effective electron-transport and hole-blocking layer in various organic electronic devices.[36–41] Its lower HOMO level of 6.7 eV is compatible with the valence band maximum of $PEA_2PbCl_1Br_3$, thereby enhancing hole-blocking efficiency within the dual ETLs device stack. Furthermore, TmPyPB's wider bandgap of 4.0 eV mitigates the spectral overlap with the perovskite emission. For the modified device architecture, we employed a dual-layer ETL comprising of 20 nm of TmPyPB and 20 nm of TPBi, as shown in Figure 2b, as compared to 40 nm of TPBi in Figure 2a. The Figure 2b device architecture led to a considerable reduction in current density at operational voltages, as evidenced by the current density measurements in Figure 2c; at 5V, the TmPyPB/TPBi device exhibited a current density of an order of magnitude lower than that of the TPBi device. The EL spectra, depicted in Figure 2d, reveals that the TmPyPB/TPBi device produces a sharp perovskite emission peak at 399 nm, in contrast to the broad emission spectrum encompassing both TPBi and perovskite for the TPBi-only device architecture (Figure 2d and S6). The strategic replacement of part of the TPBi layer with TmPyPB effectively suppresses exciton formation in the TPBi layer and promotes exciton recombination within the perovskite layer, culminating in the observed clean, single-peak EL emission.

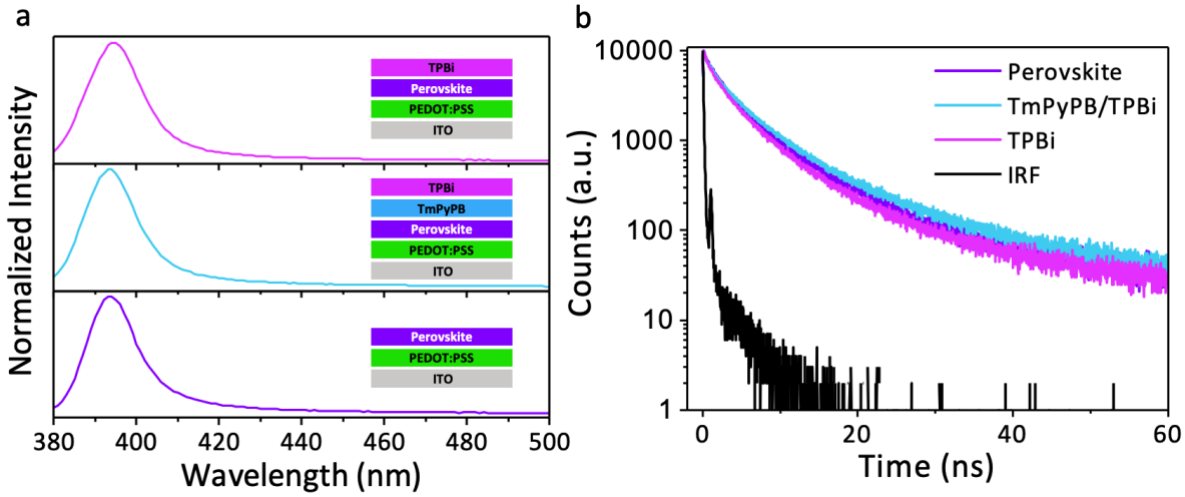

Figure 3. Optical measurements for three different device architectures.
a. PL spectra of perovskites with different electron transport layers. The inserts show the diagrams of the measured samples.
b. Time-resolved photoluminescence decay curves of perovskites with different electron transport layers.

Optical measurements were also employed to further analyze the influence of different device architectures on the optical properties of the perovskite. As depicted in Figure 3a, three distinct device structures— ITO / PEDOT: PSS / Perovskite, ITO / PEDOT:PSS / Perovskite / TmPyPB / TPBi, and ITO / PEDOT: PSS / Perovskite / TPBi —exhibited identical PL spectra when excited with a 365 nm lamp. To delve deeper, time-resolved photoluminescence (TRPL) was conducted

using a 379 nm pulsed laser to excite the devices, where the 393 nm emission was monitored. Note that TPBi PL was not observed under 365 nm or 379 nm excitations. The TRPL data, presented in Figure 3b alongside the instrument response function (IRF), were modeled using a bi-exponential decay function:

$$I(t) = A_1 \exp\left(-\frac{t}{\tau_1}\right) + A_2 \exp\left(-\frac{t}{\tau_2}\right)$$

where A_1 and A_2 are the amplitudes for the PL decay time of τ_1 and τ_2. *I(t)* is the intensity of the PL. The fitted parameters are summarized in Table 1. The PL decay of the perovskite / TPBi sample had a relatively short average PL lifetime ($\tau_{ave} = 3.28\,ns$) than the perovskite-only sample ($\tau_{ave} = 3.76\,ns$), indicating that TPBi introduced luminescence quenching for the perovskite. The perovskite / TmPyPB / TPBi sample, however, it showed the longest PL lifetime ($\tau_{ave} = 4.04\,ns$) among the three samples in Table 1, implying that TmPyPB is more effective in mitigating non-radiative recombination, potentially due to its energy level alignment with the perovskite, which helps to confine charge carriers within the perovskite layer.

Table 1: Summary of fitted parameters for TRPL measurements.

Materials	**A_1**	**τ_1(ns)**	**A_2**	**τ_2(ns)**	**R-squared**	**τ_{ave} (ns)**
Perovskite	5319.7 (52.4%)	1.60	4829.8 (47.6%)	6.14	99.90%	3.76
Perovskite/TmPyPB/TPBi	5128.3 (52.2%)	1.55	4701.6 (47.8%)	6.75	99.89%	4.04
Perovskite/TPBi	5349.5 (51.6%)	1.21	5025.3 (48.4%)	5.48	99.88%	3.28

Evaluation of UV PeLED Performance

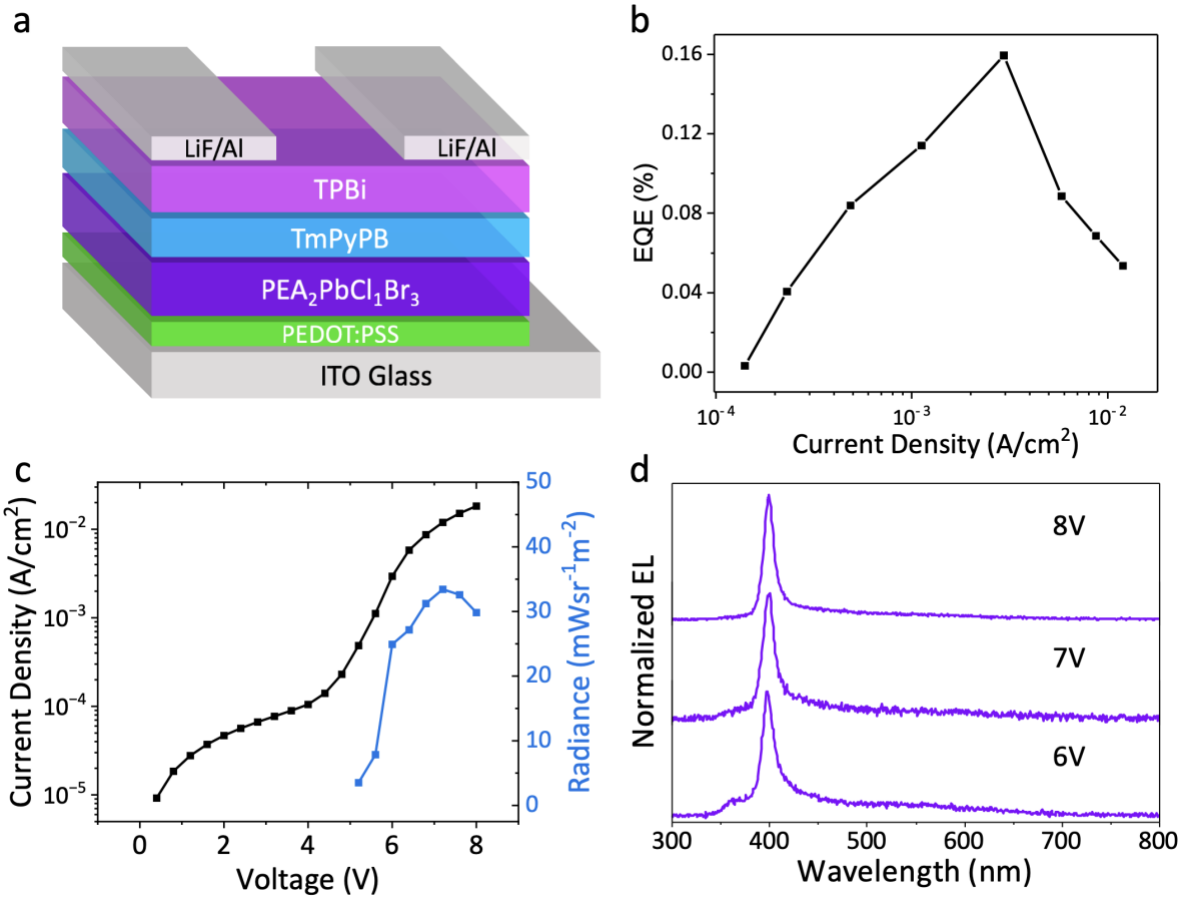

Figure 4. Dual ETLs PeLED performance.
a. Cross section diagram of the dual ETLs PeLEDs.
b. EQE – current density characteristics of the champion dual ETL PeLED.
c. Current density – voltage – radiance characteristics of the champion dual ETL PeLED.
d. EL spectra under different operating voltages.

Finally, we fabricated a series of dual ETL PeLEDs with the structure quartz / ITO / PEDOT: PSS / $PEA_2PbCl_1Br_3$ / TmPyPB / TPBi / LiF / Al, as shown in Figure 4a. Scanning electron microscopy (SEM) of the cross section of the device is shown in Figure S7. PEDOT: PSS was spin-coated on quartz ITO substrates, and the perovskite was spin-coated on top of PEDOT: PSS. The substrates were then transferred to a vacuum chamber for thermal evaporation where 20 nm of TmPyPB, 20 nm of TPBi, 2 nm of LiF and 100 nm of Al were thermally evaporated sequentially. More fabrication details can be found in the Methods section. According to the previous two-step annealing, we can also obtain 2D perovskite thin films with good coverage and crystallization, which was shown in atomic force microscopy (AFM) in Figure S8.

The EQE-current density curves, and current density – voltage – radiance curves of our champion devices are shown in Figure 4b and 4c. Our dual ETLs PeLEDs achieve a peak EQE of 0.16% at 2.9 mA/cm^2 with an average EQE of 0.08% over 58 devices (Figure S9). At voltages > 5.2 V, the

device turned on and reached its maximum radiance of 33 $mWsr^{-1}m^{-2}$ at 7.2 V. We did not observe any major change in the EL spectra across a range of operating voltages from 6 to 8 V, with only a small shoulder visible at 6 V. At 6 V, the electric field across the PeLEDs may not be strong enough for electrons to overcome the energetic barriers at the interfaces effectively leading to excitons forming in TPBi.

As shown in Figure 4d, the EL shows a dominant peak at 399 nm with a FWHM of 14 nm. We also conducted a detailed analysis of the EL spectra of devices over time, employing a constant current bias of 10 mA/cm^2 in an ambient atmosphere. The results, depicted in Figure S10a, show that the EL spectra remains stable throughout the measurement duration, indicating consistent emission characteristics under the given operational conditions. However, a critical aspect noted in our observations is the limitation of device operational lifetime, as evident from the T_{50} value being less than one second (refer to Figure S10b). This short operational duration emphasizes the necessity for further research focused on enhancing UV PeLED operational stability.

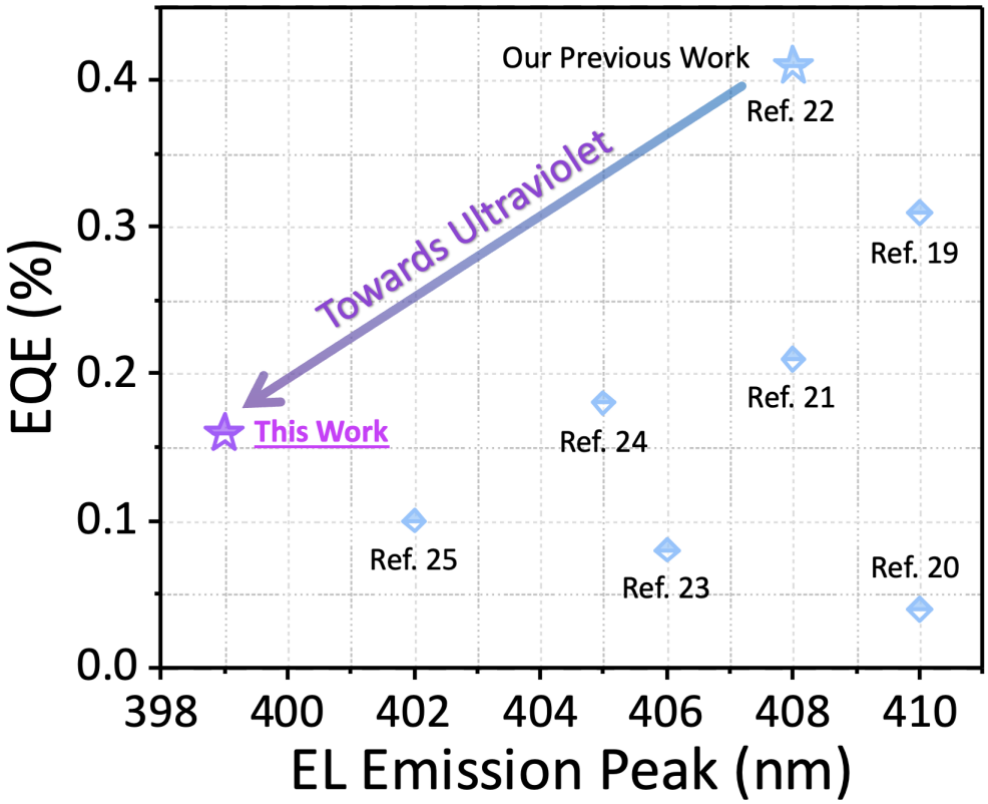

Figure 5. Summary of solution-processed lead-halide PeLEDs in the violet and ultraviolet regions.

Figure 5 presents a comprehensive overview of the performance benchmarks for solution processed violet PeLEDs reported to date. This work demonstrates the emergence of emissive perovskites for the ultraviolet regime, highlighting the potential of wide bandgap perovskite materials. Notably, this advancement also delivers an external quantum efficiency (EQE) that is highly competitive with the best-performing violet-emitting PeLEDs.

Conclusions

This investigation into the optoelectronic properties of the mixed halide 2D perovskite material $PEA_2PbCl_1Br_3$ has yielded significant insights into the complex mechanisms governing their performance in PeLEDs. The introduction of TmPyPB as an additional electron transport layer enhances charge carrier confinement and reduces non-radiative losses, as evidenced by both optical measurements and electronic device analysis. Our work culminates in the successful demonstration of solution processed PeLEDs with ultraviolet emission below 400 nm, surpassing the spectral limitations of previously reported devices while achieving reasonable EQE values. These findings not only highlight the potential of 2D perovskites in next-generation optoelectronics but also pave the way for further exploration into novel device architectures and material compositions, with the ultimate goal of realizing highly efficient, stable, and commercially viable ultraviolet electroluminescent devices.

Methods:

Materials

Phenethylammonium chloride (PEACl, >98%), phenethylammonium bromide (PEABr, >98%), and lead(II) bromide ($PbBr_2$, >99.999%) were purchased from Sigma-Aldrich. Anhydrous dimethyl sulfoxide (DMSO, ≥99.9%), anhydrous N,N-dimethylformamide (DMF, 99.8%) and anhydrous lithium fluoride (LiF, ≥99.99%) were purchased from Sigma-Aldrich. Poly(3,4-ethylenedioxythiophene)polystyrene sulfonate (PEDOT:PSS, Clevios Al 4083) was purchased from Heraeus. 2,2′,2″-(1,3,5-benzinetriyl)tris(1-phenyl-1H-benzimidazole) (TPBi, >99.5%) and 1,3,5-tri (m-pyrid-3-yl-phenyl)benzene (TmPyPB, >99.5%) were purchased from Ossila. Al (99.99%) pellets were purchased from Kurt J. Lesker Company. All chemicals were used directly as received.

Perovskite precursor

The perovskite precursor preparation was conducted inside a nitrogen-filled glovebox at room temperature. 0.1M $PEA_2PbCl_1Br_3$ stock solution was prepared by dissolving stoichiometric PEACl, PEABr, and $PbBr_2$ in DMSO then left under continuous stirring for 2 hours. The precursor solution was then filtered with a 0.22 μm PTFE syringe filter before spin coating.

Perovskite LED fabrication

The patterned-ITO coated quartz substrates (ITO resistance: 20 Ω/square, Qingdao Vatti Glass Co., Ltd) were sequentially solvent cleaned via sonication in ultra-pure water (Millipore Sigma MilliQ Ultrapure Water Purification System) with 2% volume of detergent (Hellmanex III), acetone, and isopropanol for 15 min respectively. These substrates were then dried under compressed air and treated with ultraviolet ozone for 15 min (Jelight UV-Ozone Cleaner) immediately before spin-coating PEDOT: PSS. The PEDOT: PSS aqueous solution was filtered with 0.22 μm PVDF syringe filter and then spin-coated onto the cleaned ITO substrates at 4,000 rpm for 60 s (with a ramp of 2000 rpm/s), followed by annealing at 150 °C for 20 min in ambient air. Next, the substrates were transferred to a nitrogen-filled glovebox. After the substrates cooled down to room temperature, 150 uL perovskite precursor was dropped onto the PEDOT: PSS film and spin-coated at 3,000 rpm with a ramp of 2,000 rpm/s for 30 s. Subsequently, the substrates were transferred to a glass petri dish containing 30 μL of DMF vapor for 60 s. The DMF treated petri dish had a resting period of

5 minutes between each substrate to ensure a DMF vapor-rich environment. The petri dish was wiped down with a dry nylon wipe before adding 30 uL of new DMF between spins. Afterward, the substrates were annealed at 70 °C for 5 min in a nitrogen atmosphere to remove any residual solvent. After the substrates cooled down to room temperature, they were moved into a high-vacuum thermal evaporation chamber housed within a nitrogen-filled glovebox where TmPyPB (20 nm), TPBi (20 nm), LiF (2 nm) and Al (100 nm) were deposited at 2, 1.5, 0.1, and 3 Å/s, respectively, under a high vacuum of approximately 8×10^{-6} mbar. The device area for all devices was 0.04 cm^2 as defined by the overlapping area of the ITO and Al electrode.

The perovskite device with a single TPBi ETL (Figure 2a) was fabricated using the above methods. However, 40 nm of TPBi was deposited replacing the 20 nm of TmPyPB. The TPBi EL device (Figure S6) was fabricated using the same PEDOT: PSS deposition techniques and subsequently 40 nm of TPBi replaced the original TmPyPB/TPBi layer. No perovskite layer was deposited.

Device characterization

Electroluminescence spectra were captured using an Ocean Insight QE Pro with voltages sourced to the device from a pre-programmed Keithley 2400. J-V-L characterizations from 0 V-10 V with a voltage scanning step of 0.4 V were performed using an HP4145A and a calibrated Thorlabs photodiode (FDS1010-CAL) mounted just above the face of the device.

Structure and optical characterizations

The AFM images were taken in ambient air by Bruker Dimension Icon ScanAsyst with PeakForce mode. The SEM images were collected on a FEI Magellan 400 XHR scanning electron microscope operating at 5 kV, 25 pA below 9 $x10^{-5}$ mbar with UC mode. The XRD data were collected using a PANalytical X'Pert PRO XRD system with Cu Ka radiation. The XPS data were collected using XPS: PHI VersaProbe 4 with a monochromatized Al (Ka) source and dual-gun neutralizing system. UPS was collected inside PHI VersaProbe 4 with an incident light energy of 21.22 eV (He I source). A bias of -10 V was applied to the sample to measure the secondary electron cut-off energy. Both spectra with and without bias was obtained. LEIPS was also conducted inside PHI VersaProbe 4 with an electron gun with band-pass filter of 4.77 eV. LEET spectra were simultaneously collected using a microcurrent meter. The PL spectra was measured with a Horiba FluoroLog-3 system with a Xe arc lamp. The PL lifetimes were measured with the same system but with a pulsed 375 nm laser. The absorption spectra were collected on the Agilent Cary 6000i UV/Vis/NIR system with transmission mode.

Data availability

The data that support the findings of this study are available from the corresponding authors upon reasonable request.

Acknowledgements

A portion of this work was performed at the Stanford Nano Shared Facilities (SNSF), supported by the National Science Foundation under award ECCS-2026822. We thank Juliet Jamtgaard for her assistance with the measurements conducted using the PHI VersaProbe 4 and for the discussions about the data analysis. M.H., J.L., N.M., and Q.Z. acknowledge the support of the Department of Electrical Engineering at Stanford University. N.M. amd W.M. acknowledges the support of Research Experience for Undergraduates (REU) Program at Department of Electrical Engineering, Stanford University. P.N. acknowledges the support of a Stanford Graduate Fellowship in Science & Engineering (SGF) as a Gabilan Fellow and the Chevron Fellowship in Energy. S.F. acknowledges the support from Stanford University as a Diversifying Academia, Recruiting Excellence (DARE) Fellow, the U.S. Department of Energy (DOE) Building Technologies Office (BTO) as an IBUILD Graduate Research Fellow, Stanford Graduate Fellowship in Science & Engineering (SGF) as a P. Michael Farmwald Fellow, and of the National GEM Consortium as a GEM Fellow. This work was performed under an appointment to the Building Technologies Office (BTO) IBUILD Graduate Research Fellowship administered by the Oak Ridge Institute for Science and Education (ORISE) and managed by Oak Ridge National Laboratory (ORNL) for the DOE. ORISE is managed by Oak Ridge Associated Universities (ORAU). All opinions expressed in this paper are the authors' and do not necessarily reflect the policies and views of the DOE, EERE, BTO, ORISE, ORAU, or ORNL.

References:

1. Amano, H. *et al.* The 2020 UV emitter roadmap. *J Phys D Appl Phys* **53**, 503001 (2020).
2. Fakharuddin, A. *et al.* Perovskite light-emitting diodes. *Nature Electronics 2022 5:4* **5**, 203–216 (2022).
3. Tan, Z. K. *et al.* Bright light-emitting diodes based on organometal halide perovskite. *Nature Nanotechnology 2014 9:9* **9**, 687–692 (2014).
4. Yang, D. *et al.* Toward Stable and Efficient Perovskite Light-Emitting Diodes. *Adv Funct Mater* **32**, 2109495 (2022).
5. Song, J. *et al.* Quantum Dot Light-Emitting Diodes Based on Inorganic Perovskite Cesium Lead Halides (CsPbX3). *Advanced Materials* **27**, 7162–7167 (2015).
6. Li, J. *et al.* Efficient all-thermally evaporated perovskite light-emitting diodes for active-matrix displays. *Nature Photonics 2023 17:5* **17**, 435–441 (2023).
7. Kim, J. S. *et al.* Ultra-bright, efficient and stable perovskite light-emitting diodes. *Nature 2022 611:7937* **611**, 688–694 (2022).
8. Cho, H. *et al.* Overcoming the electroluminescence efficiency limitations of perovskite light-emitting diodes. *Science (1979)* **350**, 1222–1225 (2015).
9. Fernández, S. *et al.* Trade-off between efficiency and stability in Mn2+-doped perovskite light-emitting diodes. *Device* **1**, 100017 (2023).
10. Zhang, J. *et al.* Ligand-Induced Cation–π Interactions Enable High-Efficiency, Bright, and Spectrally Stable Rec. 2020 Pure-Red Perovskite Light-Emitting Diodes. *Advanced Materials* **35**, 2303938 (2023).
11. Kim, Y. H. *et al.* Comprehensive defect suppression in perovskite nanocrystals for high-efficiency light-emitting diodes. *Nature Photonics 2021 15:2* **15**, 148–155 (2021).
12. Jiang, J. *et al.* Red Perovskite Light-Emitting Diodes with Efficiency Exceeding 25% Realized by Co-Spacer Cations. *Advanced Materials* **34**, 2204460 (2022).
13. Bai, W. *et al.* Perovskite Light-Emitting Diodes with an External Quantum Efficiency Exceeding 30%. *Advanced Materials* **35**, 2302283 (2023).
14. Zhou, W. *et al.* Manipulating Ionic Behavior with Bifunctional Additives for Efficient Sky-Blue Perovskite Light-Emitting Diodes. *Adv Funct Mater* **33**, 2301425 (2023).
15. Liu, B. *et al.* Lattice strain modulation toward efficient blue perovskite light-emitting diodes. *Sci Adv* **8**, 138 (2022).
16. Chu, S. *et al.* Large-Area and Efficient Sky-Blue Perovskite Light-Emitting Diodes via Blade-Coating. *Advanced Materials* **34**, 2108939 (2022).
17. Xing, J. *et al.* Color-stable highly luminescent sky-blue perovskite light-emitting diodes. *Nature Communications 2018 9:1* **9**, 1–8 (2018).
18. Jiang, Y. *et al.* Spectra stable blue perovskite light-emitting diodes. *Nature Communications 2019 10:1* **10**, 1–9 (2019).
19. Deng, W. *et al.* 2D Ruddlesden–Popper Perovskite Nanoplate Based Deep-Blue Light-Emitting Diodes for Light Communication. *Adv Funct Mater* **29**, 1903861 (2019).
20. Liang, D. *et al.* Color-Pure Violet-Light-Emitting Diodes Based on Layered Lead Halide Perovskite Nanoplates. *ACS Nano* **10**, 6897–6904 (2016).
21. Ma, Z. *et al.* Electrically-Driven Violet Light-Emitting Devices Based on Highly Stable Lead-Free Perovskite Cs3Sb2Br9 Quantum Dots. *ACS Energy Lett* **16**, 385–394 (2020).
22. Hu, M. *et al.* Water additives improve the efficiency of violet perovskite light-emitting diodes. *Matter* **6**, 2356–2367 (2023).

23. Chu, Z. *et al.* Centimeter-Scale Violet Light Emitting Diode with Two-Dimensional BA2PbBr4 Perovskite Emitter. *J Electrochem Soc* **170**, 065501 (2023).
24. Zhang, C. *et al.* Narrow-Band Violet-Light-Emitting Diodes Based on Stable Cesium Lead Chloride Perovskite Nanocrystals. *ACS Energy Lett* **6**, 3545–3554 (2021).
25. Hu, Q. *et al.* Efficient and Stable Mg2+-Doped CsPbCl3Nanocrystals for Violet LEDs. *Journal of Physical Chemistry Letters* **12**, 8203–8211 (2021).
26. Hu, M., Murrietta, N., Lyu, J. & Congreve, D. N. Two-dimensional perovskite materials towards violet and ultraviolet light-emitting diodes. in *UV and Higher Energy Photonics: From Materials to Applications 2023* (eds. Lérondel, G., Cho, Y.-H. & Taguchi, A.) 6 (SPIE, 2023). doi:10.1117/12.2676613.
27. Crace, E. J., Su, A. C. & Karunadasa, H. I. Reliably obtaining white light from layered halide perovskites at room temperature. *Chem Sci* **13**, 9973–9979 (2022).
28. Han, Y. *et al.* Exciton Self-Trapping for White Emission in 100-Oriented Two-Dimensional Perovskites via Halogen Substitution. *ACS Energy Lett* **7**, 453–460 (2022).
29. Elleuch, S., Lusson, A., Pillet, S., Boukheddaden, K. & Abid, Y. White Light Emission from a Zero-Dimensional Lead Chloride Hybrid Material. *ACS Photonics* **7**, 1178–1187 (2020).
30. Terashima, M. *et al.* The electronic band structure analysis of OLED device by means of in situ LEIPS and UPS combined with GCIB. *Surface and Interface Analysis* **52**, 948–952 (2020).
31. Hikima, K. *et al.* Operando analysis of electronic band structure in an all-solid-state thin-film battery. *Communications Chemistry 2022 5:1* **5**, 1–9 (2022).
32. Shen, Y. *et al.* Interfacial Potassium-Guided Grain Growth for Efficient Deep-Blue Perovskite Light-Emitting Diodes. *Adv Funct Mater* **31**, 2006736 (2021).
33. Zou, G. *et al.* Color-Stable Deep-Blue Perovskite Light-Emitting Diodes Based on Organotrichlorosilane Post-Treatment. *Adv Funct Mater* **31**, 2103219 (2021).
34. Yan, S. *et al.* Deep Blue Layered Lead Perovskite Light-Emitting Diode. *Adv Opt Mater* **9**, 2001709 (2021).
35. Zhang, J. *et al.* A Multifunctional "Halide-Equivalent" Anion Enabling Efficient CsPb(Br/I)3 Nanocrystals Pure-Red Light-Emitting Diodes with External Quantum Efficiency Exceeding 23%. *Advanced Materials* **35**, 2209002 (2023).
36. Chen, Y., Chen, J., Zhao, Y. & Ma, D. High efficiency blue phosphorescent organic light-emitting diode based on blend of hole- and electron-transporting materials as a co-host. *Appl Phys Lett* **100**, 213301 (2012).
37. Shi-Jian Su, B. *et al.* Pyridine-Containing Triphenylbenzene Derivatives with High Electron Mobility for Highly Efficient Phosphorescent OLEDs. *Advanced Materials* **20**, 2125–2130 (2008).
38. Lee, H. *et al.* Highly efficient green, blue, and white phosphorescent inverted organic light-emitting diodes by improving charge injection and balance. *J Mater Chem C Mater* **5**, 9911–9919 (2017).
39. Wang, S. *et al.* Solution-Processed Phosphorescent Organic Light-Emitting Diodes with Ultralow Driving Voltage and Very High Power Efficiency. *Scientific Reports 2015 5:1* **5**, 1–9 (2015).
40. Wu, S., Li, S., Sun, Q., Huang, C. & Fung, M. K. Highly Efficient White Organic Light-Emitting Diodes with Ultrathin Emissive Layers and a Spacer-Free Structure. *Scientific Reports 2016 6:1* **6**, 1–8 (2016).

41. Fan, C. *et al.* Using an Organic Molecule with Low Triplet Energy as a Host in a Highly Efficient Blue Electrophosphorescent Device. *Angewandte Chemie International Edition* **53**, 2147–2151 (2014).